Curvature defects in lamellar phases of amphiphile–water systems

Carey K. Bagdassarian
Department of Chemistry, University of California, Los Angeles, California 90024

Didier Roux
Centre de Recherche Paul Pascal–Centre National de la Recherche Scientifique, Universite de Bordeaux, Pessac 33600, France

Avinoam Ben-Shaul
Department of Physical Chemistry, Fritz Haber Center for Molecular Dynamics, The Hebrew University, Jerusalem 91904, Israel

William M. Gelbart
Department of Chemistry, University of California, Los Angeles, California 90024

(Received 6 July 1990; accepted 6 November 1990)

Within the framework of two complementary models, we show that the densities and patterns of defects in amphiphile–water systems with lamellar organization are coupled to the strength of the bilayer–bilayer interactions and hence to the overall surfactant concentration. We consider defects which introduce curvature (i.e., larger head-group area per molecule) while preserving the integrity of stacked bilayers at surfactant volume fractions of several tenths. These features are favored if the molecules comprising the lamellae are preferentially packed with a *non*planar aggregate–water interface: curvature defects lower the *local* free energy in systems constrained by aggregate–aggregate interactions to lamellar geometry. As the amphiphile volume fraction is increased—and the bilayer–bilayer spacing thereby decreased—we predict phase transitions between lamellar phases of different defect patterns on the bilayer surface, with concurrent decrease in the defect area fraction per bilayer. Specifically, there is a progression from a stripe-like pattern of parallel channels to a random network of line defects to a pore phase, with the latter appearing at the highest amphiphile concentrations but characterized by the lowest density of defects. Connection is made with experimental work which has recently suggested various departures from classical lamellar structure.

I. INTRODUCTION

The lamellar phase of an amphiphile–water system is characterized by alternating, stacked sheets of bilayer and water domains. The bilayers have traditionally been thought of as continuous, homogeneous structures (membranes), but recent experimental work indicates that they are actually pierced by pores or channels which allow for water in the planes of the membranes.[1–6] In this paper we investigate the coupling to amphiphile concentration of the densities and patterns of these lamellar defects. These defects serve to introduce local curvature, the nature of which will be made explicit shortly, into otherwise planar lamellae; accordingly, they should be favored in bilayers formed by molecules preferring a curved aggregate–water interface.

We begin with a brief review of the phase diagrams of these surfactant systems in order to expose the driving force for defect formation in these planar bilayer systems.

An amphiphile, or surfactant molecule, consists of a hydrophilic head group which can be ionic, polar, or zwitterionic, and a hydrophobic tail, consisting of one or two alkyl chains. Understanding their aqueous solution phase diagrams[7] presents a rich challenge because the aggregates formed by these molecules do not maintain their integrity as colloidal particles; instead they respond via shape and size reorganization to changes in temperature and concentration. More explicitly, below what is called the critical micellar concentration (CMC), the surfactant molecules are soluble as monomers in aqueous solution. Above the CMC, self-assembly—driven by the hydrophobic effect—organizes the system into small aggregates. At low enough concentrations, where aggregate–aggregate interactions can be ignored, these colloidal particles behave as an ideal solution; even so, their shapes and sizes are dependent upon competition between molecular packing constraints and the translational entropy of the particles.[8] Specifically, entropy favors a large number of small, globular micelles, while the packing constraints involve a molecular preference for a given geometrical environment, e.g., that of a sphere, cylinder, or planar bilayer, say. Because the head groups shield water from the hydrocarbon tails, they are found to cover the surface of any aggregate formed; for interfaces with positive curvature each hydrophilic moiety has a larger area than its chain.

This molecular preference for a given curvature (spherical, cylindrical, or planar) will be crucial in our work, and we concentrate on molecules having their local free energies minimized by a *cylindrical* geometry—that is, the surfactant of interest will have an optimal head-group area which is larger than the cross-sectional area of its tail. For these amphiphiles, then, we find, in the dilute regime, an isotropic solution of rod-like aggregates whose lengths are concentration dependent. At higher surfactant mole fractions, interaggregate interactions trigger first an isotropic-nematic transition and then a hexagonally packed phase of infinite cylinders.[9] On the other hand, if the surfactant strongly

 0021-9606/91/043030-12$03.00

prefers the larger curvature of a spherical interface, the system may undergo a direct transition from an isotropic phase of spheres to a nematic state of rods,[10] which underscores, again, the importance of molecular constraints. In either case, the onset of long-range orientational order results from interaggregate interactions. Upon further increase in surfactant concentration, reorganization into a translationally ordered system of amphiphilic bilayers, the lamellar phase, takes place. This phase, in principle, can be packed to a surfactant volume fraction of unity. An example of a surfactant showing an isotropic–hexagonal–lamellar phase progression is dodecyltrimethylammonium chloride.[11]

It is clear that lamellae satisfy global, *aggregate* (vs local, *molecular*) packing requirements at the moderately high surfactant volume fractions of several tenths, since such planar aggregates relieve the "grid-lock" (i.e., less-efficient packing) of a concentrated hexagonal phase. On a *molecular* level though, there is a free-energy price for packing the molecules in a planar bilayer: the molecules prefer a cylindrical aggregate–water interface and the bilayer does not provide the necessary curvature. In the present work, we consider a simple way to introduce curvature into the membrane without destroying its overall planar geometry, the "motivation" being to allow at least some of the surfactant molecules in the bilayer to enjoy locally a more curved environment. This is done by introducing defects such that a molecule residing in the defect will have a lower free energy than one on the planar surface, consistent with the idea that *molecular* packing constraints can be better satisfied when the amphiphiles reside in a curved geometry. We concentrate upon *in*-plane defects which are uncorrelated between successive layers.

Pertinent experimental work has focused on lamellar phases (L_α) lying close to nematic or hexagonal ones. For example, the decylammonium chloride/water/ammonium chloride system studied by Holmes and Charvolin[1] exhibits, at low temperature, a lamellar phase which upon heating (at constant surfactant concentration) transforms into a nematic phase of discotic micelles. It is found that L_α consists of bilayers containing pores or channels, which mediate transition to the discotic nematic. A similar conclusion is drawn by Chidichimo *et al.* for a water/ammonium perfluorononanoate system.[2] Holmes, Reynolds, and Boden,[3] for a cesium pentadecafluorooctanoate/water mixture, show that the lamellar phase itself (close lying to a discotic) consists of discoid micelles—certainly a curvature-adding defect situation. Indeed, the common lamellar phase of SdS/water (where SdS denotes sodium decyl sulfate) shows diffuse neutron scattering indicating defects which, at low temperatures and low surfactant fraction, are correlated between adjacent bilayers; with increasing temperature and concentration the defects remain correlated *within*—but not *between*—bilayers.[4] Finally, Kekicheff and Tiddy[5] find an interesting phase transition in the lithium perfluorooctanoate/water system where, at low temperatures and high surfactant fraction, there exists an "intermediate" phase which is lamellar with strongly correlated defects staggered from one layer to the next. Upon heating, an L_α phase appears which shows a loss of these interplane defect correlations

Although within the framework of our theory we focus on uncorrelated in-plane defects which do not alter the planar nature of the lamellae, these are not the only defects observed. Freeze-fracture electron microscopy has revealed various defect structures in lamellar phases of lipids, such as confocal domains, screw dislocations, and disclinations.[12] Theoretical work aimed at characterizing and understanding such structures is extensive.[13–15] Sadoc and Charvolin[16] have used geometric ideas to explain defect formation as a result of frustration in bilayers. Lamellar phases of nonionic surfactants, such as hexaethylene glycol dodecyl ether ($C_{12}E_6$), exhibit a temperature-dependent, defect-mediated phase transition in which the bilayers are disrupted by dislocation loops.[17,18] Ripple phases[19–22] also serve to introduce modulated curvature into the lamellar systems, and these defects add a negative contribution to the free energy. Finally, Petrov, Mitov, and Derzhanski consider saddle splay instabilities and the presence of pores in bilayers.[23,24] It is clear that all of these defects alter the classical lamellar structure.

We propose here two complimentary models which allow description of the topology of in-plane defects, that is, the pattern of defects in a bilayer. As will be made explicit below, the first model builds up patterns, on the bilayer surfaces, from random lines of defect, with the defect playing the role, in two-dimensions, of the surfactant film in microemulsion structures. The second model allows for growth of pore defects into finite strips or channels, analogous to micellar growth in the dilute surfactant regime. In each case, the amount of defect is coupled to the surfactant volume fraction: we find that the area fraction of defect per bilayer decreases with increasing surfactant concentration. With this decrease in defect density, the surface patterns change, and we predict phase transitions (first and second order) between lamellar phases with different defect patterns. In other words, we relate the topology and the amount of defect within a membrane to the bilayer–bilayer interactions.

II. CURVATURE DEFECTS, BILAYER–BILAYER INTERACTIONS, AND LAMELLAR GEOMETRY

Before the two models are presented in the following section, it will prove useful to state the general, model-independent features upon which our ideas are built. As discussed above, we envision the bilayers in a lamellar phase to contain defects which introduce curvature into an otherwise planar system. The simplest of these is a *pore* (see Fig. 1). The curvature is added via the inner surface of a toroidal "lip" which "heals" the defect in the sense that the surfactant molecules on this surface shield otherwise exposed hydrophobic tails from the aqueous surroundings. If the radius of the pore is sufficiently large, the head groups enjoy a region of overall positive curvature on the defect surface. One of the principal curvatures is certainly negative—meaning that the head groups along the direction are more closely packed than in a flat surface—but this negative curvature can be made small with a large pore size. Other defect geometries, e.g., *lines*, can add curvature as well, and here we will need to differentiate between the patterns allowed by each of the models; the patterns shown in Fig. 2(a) correspond to the first, random line, model, while those in Fig. 2(b) are for the defect growth model.

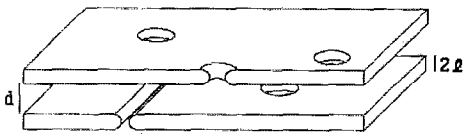

FIG. 1. Lamellar geometry showing line and pore defects of curvature. We stress that our theories do not allow for coexistence of lines and pores within the same bilayer: we simply illustrate here ways in which curvature is added to a lamella.

Looking down upon a bilayer face, one can imagine a *stripe phase* [see leftmost picture in Fig. 2(a)] in which narrow, parallel channels run the length of the bilayer: we have a phase of parallel lines. On the other hand, as in the second model, these parallel channels may be of *finite* length with the pattern corresponding to a translationally disordered *nematic phase of channels* in two dimensions [see leftmost picture in Fig. 2(b)]; this is the first instance where a qualitative difference arises between our two models. Furthermore, in both models these channels may form a random network, which we will call a *random line* phase for the first and an *isotropic* phase for the second, with bends or crossings (we discuss this distinction below) in the building-block line defects (center pictures in Figs. 2(a) and 2(b)]. Figure 1 shows the nature of these channels: they are healed by half-cylindrical lips with, for simplicity, a constant defect width (lip–lip separation) a. It should be noted that we have chosen our surfactants so that they prefer the local packing geometry of these half-cylindrical lips and that, for a fixed-area fraction of defects per bilayers, these narrow channels allow a maximum number of molecules to enjoy such regions of higher curvature—that is, the channels maximize the length of the cylindrical defect surfaces. Figure 2(a)[2(b)] shows progression from stripe (nematic) to random line (isotropic) to pore phases—it will be seen that this pattern sequence, in the direction of increasing surfactant concentration, is determined by the statistical thermodynamics of the problem.

Note that these healing surfaces are simply *mono*layers of surfactant curved back on themselves with radius of curvature on the order of a molecular length. In this fashion, defect energies can be related to monolayer elastic bending energies. Indeed, if a monolayer made of amphiphile of a particular type has a relatively large spontaneous curvature, in the direction of larger head groups, it would be reasonable to expect that a line defect (with its half-cylindrical lip) would be energetically favored—more so than a pore, say, which involves in addition a *negative* curvature. Defect energies will be treated phenomenologically in our work, with connection made to the bending constants of a surfactant film (monolayer).

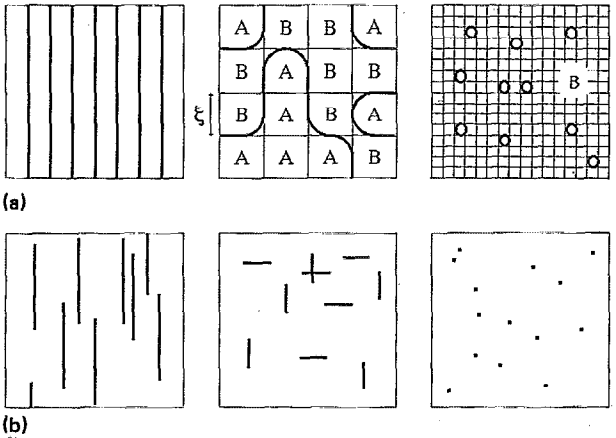

FIG. 2. (a) Stripe–random-line–pore progression, with increasing surfactant volume fraction (decreasing defect density), within the line defect model. (b) Nematic–isotropic–pore progression, with decreasing defect area fraction, described by the defect growth model.

Having introduced curvature defects as a means of lowering the *local* free energy of surfactant packing, we must consider the way in which *inter*bilayer interactions serve to suppress their proliferation. Qualitatively, it suffices to use any *repulsive* interaction between the stacked lamella: electrostatic, screened electrostatic, Helfrich undulation, or hydration forces will lead to the same picture.[25] In this work we use an electrostatic interaction between the bilayers (consisting of ionic surfactant) with a subsequent generalization independent of the details of the interaction. Now, "creation" of a pore, say, involves the removal of a block of molecules from the membrane. These "extra" molecules can be used either to thicken existing bilayers or to form new bilayers. In either case, the surface–surface distance between opposing, interacting, lamellae is decreased with resulting increase in the repulsive force between these surfaces. It is therefore expected that defect formation raises the *interaction* free energy above that of perfect bilayers at the same volume fraction: bilayer–bilayer interactions serve, therefore, as a "brake" on defect number, or more conveniently, defect area fraction per bilayer. It is also appreciated that these interactions become more important at high surfactant volume fraction (when the bilayers are anyhow closer together), and we expect, with increasing amphiphile concentration, a decrease in the amount of defect. Hence, defects are lost upon concentration of lamellar phases (Kekicheff and Tiddy[5] allude to this), and an essentially "perfect" bilayer results.

We now investigate what can be learned from the geometry of the lamellar phase (see Fig. 1), pursuing as long as we can ideas which are model independent. A given bilayer is taken to be of thickness $2l$ and facial area L^2. If we demand, for simplicity, that the introduction of defects into the membranes only increases the number of bilayers and not their thickness, we have a constant area per head group, call it Σ, and, of course, a constant membrane thickness $2l$. This condition can be relaxed but Σ would then have to be treated as a variational parameter. This area per head group refers to a surfactant molecule in the bilayer proper, rather than in the defect (where we expect a larger value). With v taken as the incompressible volume per molecule, a simple relation is obtained from the bilayer geometry which holds in the presence or absence of defects:

$$\Sigma = v/l. \tag{1}$$

(For comparison, in the half-cylindrical lip of a channel the area per head group is $2v/l$.)

A most important *variational parameter* is ϕ_d, the area

fraction of defect—that is, the fraction of the bilayer surface covered with defect, independent of pattern. It is just this quantity, ϕ_d, that decreases with increasing surfactant volume fraction, as described above. Since L^2 is the area of a single face of bilayer, it is clear that the number of surfactant molecules per bilayer (with neglect of the number used to heal the defects) is

$$2L^2(1-\phi_d)/\Sigma. \tag{2}$$

This relation serves also to define the area fraction ϕ_d. Though we have suppressed details of the healing lips by neglecting to count the number of molecules in them (which is small for small ϕ_d), we capture the main idea of defect introduction: as ϕ_d increases, the number of molecules in each membrane decreases, but new lamellae are necessarily formed (at fixed surfactant fraction). Finally, if d is the *inter*lamellar spacing (actually, the distance between bilayer surfaces) and ϕ the surfactant volume fraction, we have

$$d = 2v(1-\phi-\phi_d)/\phi\Sigma. \tag{3}$$

Clearly, as ϕ_d increases, for fixed ϕ, the distance d decreases.

III. DEFECT MODELS

A. Line defect model

1. Description of model

We present the first (line defect) model, develop the corresponding free energy (Secs. III A 2 and III A 3), and work out a representative phase diagram (Sec. III A 4). The second (defect growth) model is subsequently described (see Secs. III B 1–III B 3 below) and the two compared. The line defect model will provide for a simple treatment of the random line phase—a random network of defects—with the pore phase as a limiting case. The stripe phase is included in a simple fashion.

Let the surface of a bilayer be partitioned into a square lattice with lattice size ξ: this will allow for calculation of defect energies and entropies via a simple scheme which also defines the topology. The formulation is motivated by the phenomenological theory of microemulsions[26–29] and especially by the description of planar surfaces in the isotropic L_3 ("sheety" or "sponge") phase of dilute surfactant solutions.[30] We divide, randomly, the lattice squares into types A and B, with ψ defined as the area fraction of A. The equilibrium value of ψ will follow from free-energy minimization for given surfactant volume fraction, ϕ. That is, ψ is the second unconstrained variable or *variational parameter* (the first being the defect area fraction ϕ_d, as discussed above). Note that A and B do not refer to different species or phases; rather, they denote different regions of the bilayer, separated by line defect (i.e., a water "crack" of width a). Correspondingly, ψ does not describe a composition, but is instead *a measure of the topological organization of defect.* We shall see shortly, in the random mixing approximation, that there is a direct relation between the lattice constant ξ and the two variational parameters, ψ and ϕ_d: for each pair ψ and ϕ_d, there corresponds a unique ξ.

At the interface of an A square and a B square we lay down our strip of line defect; again, the defect is transmembrane (a channel) but we are now concerned only with the surface features of the bilayer. Figure 2(a) shows typical patterns constructed from the model. The defects are pictured as self-avoiding at positions of possible crossings. We choose to exclude crossings because the surfactant molecules in them would not have the preferred cylindrical packing. As such, crossings are energetically unfavorable with respect to the gently bending patterns replacing them. Furthermore, the line defect model does not allow for lines that simply "end"—the allowed defect patterns are closed. Indeed, the surfactant head groups in an end, if it were possible, would have an area per molecule smaller than those in the pores as they arise in this model. Energetically, then, ends can be excluded. Accordingly, for the self-avoiding case, the building block of all defect patterns is the line defect and the corresponding energy is described by a single quantity, the defect energy per unit length. Furthermore, the paired-lip (separated by a distance a) nature leads to a particularly simple form for this quantity. [Our second model (see Sec. III B) will allow for free ends and crossings (if desired) but with an associated price.]

If $\mathscr{L}$ is taken to be the total length of defect per bilayer, as measured by the length of the A–B interface, then

$$\mathscr{L} = 4N\psi(1-\psi)\xi \tag{4}$$

in the random mixing approximation. Here $N = L^2/\xi^2$ is the number of squares in the lattice, ψ is the probability of an A square, and $1-\psi$ of a B square. Since all defects are of width a, $\phi_d = \mathscr{L}a/L^2$, and from (4) and $N = L^2/\xi^2$ we have

$$\xi = 4a\psi(1-\psi)/\phi_d. \tag{5}$$

This is, of course, analogous to the expression used in the microemulsion work, with ϕ_d corresponding to the volume fraction of surfactant, ψ to the volume fraction of, say, oil, and $1-\psi$ to that of water. In the microemulsion case, however, both ϕ_d and ψ are *fixed* by composition, whereas in our equation (5), *both* of these are unconstrained variables (and, as stated, determine ξ): the statistical thermodynamic free energies which we will obtain are then minimized with respect to these two quantities.

Equation (5) immediately suggests a natural cutoff value for ξ which serves to effectively define a pore phase. More explicitly, as ψ decreases, the defects become loops around isolated A squares. Concurrently, with decreasing ψ, ξ decreases for fixed area fraction of defect and, if the lower cutoff is taken as $\xi \equiv a$, we find a phase of isolated pore-like defects each of area a^2. On the other hand, if ψ and ξ turn out to be larger, with $\psi = 1/2$ as the maximum, an extended network of line defects is realized. Figure 2(a) depicts these extremes. For convenience, we refer to the $\psi = 1/2$ situation as a *random line phase* and the $\psi < 1/2$ phase as a *pore phase*, even though we may be far away from the pore cutoff described.

In order to determine the defect energies it will be necessary to count the number of bends in the length $\mathscr{L}$ of the defect. This is done in the random mixing approximation, with the realization that each of the four appropriate configurations of A–A–A–B squares and each of four arrange-

ments of B–B–B–A squares is associated with a bend, while two bends (because of self-avoidance) are associated with each of the two pertinent configurations of A–B–A–B squares [examples can easily be found in Fig. 2(a)]. Since the bends occur at the vertices of the lattice, of which there are N (the number of squares), we have for the total number of bends:

$$4N\psi^3(1-\psi)+4N\psi(1-\psi)^3+4N\psi^2(1-\psi)^2 = \frac{4L^2}{\xi^2}\psi(1-\psi)[1-\psi(1-\psi)] \approx \frac{4L^2}{\xi^2}\psi(1-\psi). \tag{6}$$

In ignoring terms in $\psi^2(1-\psi)^2$ compared with $\psi(1-\psi)$, we essentially ignore any special interaction energy for the self-avoiding defect pairs whose number goes with $\psi^2(1-\psi)^2$.

2. Free-energy considerations

The total free energy of the lamellar phase is given by the free energy per bilayer multiplied by the number of bilayers, with the latter not constant during the variation with respect to ϕ_d. As was seen, the two-dimensional aspect of the defect density is coupled to the overall three-dimensional nature of the lamellar system: as ϕ_d increases, the number of bilayers increases. It is appropriate, then, to minimize with respect to ϕ_d and ψ a free-energy density defined by the total free energy divided by the total volume. Actually, it is convenient to define an intensive free energy defined by the product of this density and the space-filling molecular volume "v." The simplest way to proceed with this quantity is to introduce a free energy per bilayer, divide by the number of molecules in it, and multiply by the surfactant volume fraction. Furthermore, a plot of this free energy vs ϕ, after the extremum values of the ϕ_d and ψ are obtained, provides the basis for a common tangent construction for locating first-order transitions between coexisting lamellar phases of different defect densities and topologies. (The coexistence is *not* between different topologies and area fractions within a *given* bilayer, but rather—in the usual way—between macroscopic domains of lamellar phases, each characterized by a specific ϕ_d, ψ, and ϕ.)

The *dimensionless* free energy will feature three contributions:

$$\frac{Fv}{k_BTV} \equiv f = f_d + f_e + f_b, \tag{7}$$

where F and V are the total free energy and volume of the system (k_B is Boltzmann's constant, T the temperature, and v the conserved molecular volume referred to above). The first term in Eq. (7) refers to the "core" defect energies which can be regarded as elastic energies associated with the curved lips. f_e is the defect entropy and is calculated via the mixing entropy of the A–B lattice, as in (13) below. Finally, f_b describes the bilayer–bilayer interaction which suppresses defect proliferation. To the extent that the area per head group, Σ, is fixed, any surface free-energy term of the type $\gamma\Sigma$ is inconsequential: it would simply have the form of a constant times ϕ, and can be ignored.

The defect energy f_d can be thought of in two ways. Because the building block of the defect pattern is a line, it is natural to introduce an energy per unit length. Phenomenologically, we can write the local elastic energy per unit length for a "line" as a function of its curvature (we ignore the defect width) as

$$-\delta+\chi C_1^2. \tag{8}$$

$-\delta$ in Eq. (8) is the core energy per unit length of the locally straight line defect. C_1 is the single curvature needed to characterize its bending and is measured along the length of the defect pattern in the bilayer plane (C_1 is nonzero only at bends). χ is a harmonic bending constant, having dimensions of energy times length. There is no term linear in the curvature since the straight line, by symmetry, corresponds to the energy minimum. Furthermore, $\chi>0$ since there is a free-energy price for bending. Now, since $-\delta$ must reflect the idea that defects provide the opportunity for molecules to pack with large head-group areas, $-\delta<0$. Indeed, the energy per unit length of Eq. (8) can be thought of as serving the role of the free-energy difference between a molecule in the defect and one in the bilayer proper. The validity of the above expression breaks down in the limit of pore defects, where we apply Eq. (8) only qualitatively. More explicitly, we write the line energy as $-\delta+\chi(aC_1)^2/a^2$ and require that $aC_1 \ll 1$: this is not the case for a pore where $C_1 \sim 1/a$. The idea, however, is clear: straight, nonbending, defects are preferred.

We can understand Eq. (8) in the context of the elastic properties of the monolayer of surfactant curved to form a defect by starting with the Helfrich[31] expression for the elastic energy per unit area of a monolayer:

$$F = F(0,0) - \tfrac{1}{2}kC_0^2 + \tfrac{1}{2}k(C_1+C_2-C_0)^2 + \bar{k}C_1C_2. \tag{9}$$

$F(0,0)$ is the energy per unit area of the locally flat monolayer and depends on the nature of the surfactant; C_0 is the spontaneous curvature. C_1 and C_2 are the two principal curvatures, with C_1 (as above) taken along the defect line as seen from above the bilayer surface, and C_2 measured along the semicircle described by the defect lip ($C_2 = 1/l$ everywhere). The elastic constants of the monolayer are k and $\bar{k}$. Briefly, Eq. (9), or more properly the quantity $F-F(0,0)$, since we need an energy difference between the defect surface and the bilayer proper, can be rewritten as an energy per unit length for a single lip and added to the corresponding quantity for the other lip, with $C_1 \Leftrightarrow -C_1$ for the pair. It follows that no linear terms in C_1 remain and that energy per unit length is

$$-2\pi kC_0 + \pi k/l + \pi klC_1^2. \tag{10}$$

Clearly, Eq. (8) is recovered with $-\delta \equiv -2\pi kC_0 + \pi k/l$ and $\chi \equiv \pi kl$. As indicated, $\chi>0$ (since $k>0$) and $-\delta$ is taken as negative in order to promote defects (and, indeed, $C_0>0$ here).

Because Eq. (8) is a local quantity, it must be integrated over the length defect. The energy becomes (recalling that $\mathcal{L} = \phi_d L^2/a$ and that $C_1 \neq 0$ only in the bends), for the bilayer,

$$F_d = \frac{-\delta\phi_d L^2}{a} + \chi C_1^2 \text{ (number of bends)(length per bend)}. \tag{11}$$

The number of bends has previously been calculated in the random mixing approximation; see Eq. (6). A bend is envisioned in the lattice model to be a quarter-circle of radius $\xi/2 = 1/C_1$. With the above result for the core defect free energy per bilayer, Eq. (6) for the number of bends per layer, and Eq. (2) for the number of surfactant molecules, the dimensionless free energy f_d becomes

$$f_d = -\frac{\delta\phi_d\phi}{1-\phi_d} + \frac{\chi a^3\psi(1-\psi)\phi}{\xi^3(1-\phi_d)}. \tag{12}$$

Here, δ and χ have been rendered dimensionless and are related to the corresponding parameters in Eq. (8) by $\delta \equiv \Sigma\delta/2ak_BT$ and $\chi \equiv 2\pi\Sigma\chi/a^3k_BT$. From Eq. (5), furthermore, $\xi = 4a\psi(1-\psi)/\phi_d$ with both ψ and ϕ_d variational parameters, and ϕ is the surfactant volume fraction.

Calculation of the entropic contribution f_e relies on the connection between the A–B mixing entropy and that of the defects. We stress that, since the A–B squares comprise a fictitious division of the bilayer surface, this scheme is simply a convenient device for arriving at f_e. To within an additive term in $\psi^2(1-\psi)^2$ (which accounts for the self-avoidance of the line defects, at sites of potential crossings, by either bending towards A squares or B squares), we find

$$f_e = \frac{a^2C\phi}{\xi^2(1-\phi_d)}[\psi\ln\psi + (1-\psi)\ln(1-\psi)] \tag{13}$$

with $C \equiv \Sigma/2a^2$ dimensionless.

The remaining contribution is the bilayer–bilayer interaction free energy. As mentioned earlier, this term is a matter of preference, and we will use the electrostatic interactions between bilayers which can be easily calculated by solving the Poisson–Boltzmann equation with the appropriate boundary conditions (see Ref. 25 and references within). We use the limit in which the free energy per bilayer goes as the inverse of the distance between the bilayers, d. Though this is a useful limit of the electrostatic interactions, we could have simply postulated that the bilayer–bilayer interactions have the form (where the free energy is for a bilayer) $F_b = AL^2/d$ since all that is required is a repulsive term. This form suggests a particularly simple and natural coupling between the defect area fraction, ϕ_d, and the surfactant concentration, ϕ. If we assume that the only effect of defect introduction is to alter the intermembrane spacing d [see Eq. (3)], then we arrive at

$$f_b = A\phi^2/(1-\phi_d)(1-\phi-\phi_d), \tag{14}$$

where A is now dimensionless and related to the corresponding quantity in F_b above by $A \equiv A\Sigma^2/4vk_BT$. At fixed surfactant volume fraction ϕ, the overall effect—since d decreases with increasing ϕ_d according to Eq. (3)—is an increase in f_b with increase in ϕ_d: this is the sense in which interbilayer interactions suppress the proliferation of defects, as discussed earlier.

We collect here the free-energy density terms, and, with ξ given by Eq. (5), find

$$f = \frac{A\phi^2}{(1-\phi_d)(1-\phi-\phi_d)} - \frac{\delta\phi_d\phi}{1-\phi_d} + \frac{\chi\phi_d^3\phi}{1-\phi_d}\left[\frac{1}{\psi^2(1-\psi)^2}\right] + \frac{\phi_d^2\phi}{1-\phi_d}\left[\frac{\psi\ln\psi + (1-\psi)\ln(1-\psi)}{\psi^2(1-\psi)^2}\right]. \tag{15}$$

We have divided f by the dimensionless coefficient of the entropic term, which is $C/4^2$ after the substitution for ξ, and have accordingly rescaled the other coefficients, A, δ and χ. This free-energy density serves to describe the symmetric ($\psi = 1/2$) random line and pore ($\psi < 1/2$) phases.

As discussed above, the stripe phase is one where the defect channels are parallel to each other throughout the bilayer surface—for such a pattern we can eliminate the bending energy given by the third term on the right-hand side of Eq. (15). We crudely describe this phase by the first two terms in the free-energy density above:

$$f_{\text{stripe}} = \frac{A\phi^2}{(1-\phi_d)(1-\phi-\phi_d)} - \frac{\delta\phi_d\phi}{1-\phi_d}. \tag{16}$$

This is easily justifiable: the stripe phase has no "topological" entropy or bending. That is, the only disorder in this phase is characterized by thermal undulations of the line defects about the basic parallel pattern. We ignore the details of these thermal fluctuations as we did in the random line and pore phases. As such, there is no need for an entropic term for any unknown topology (as there is in the other phases), and there are no bends in this topological sense. In the absence of these fluctuations, we would just need a one-dimensional entropy which would characterize the nonperiodicity of the stripes—a quantity that scales with the length of the bilayer and is, therefore, negligible compared to the other free-energy components (per bilayer) which scale with the area (length squared).

3. Qualitative discussion and simplification of the free-energy density

Much can be learned by inspection of Eq. (15). The area fraction of defect, ϕ_d, is controlled essentially by the first two terms in the free-energy density—that is, the features of the stripe-phase free energy determine ϕ_d. This is because the bending and entropic terms are higher order in ϕ_d than the second, core-energy term. Furthermore, the coefficient A as calculated from the electrostatics or as simply chosen, is large enough so that the linear term in ϕ_d contained within the interaction free energy will dominate over the bending and entropic contributions at moderate values of ϕ. The electrostatic interaction term is minimized by $\phi_d = 0$ (at fixed ϕ) while $\delta > 0$ allows for the defects to "grow in" (i.e., favors large ϕ_d). The *topology* of the defects (cf. ψ), for fixed ϕ_d, is controlled by the last two terms of the free energy. Since $\chi > 0$, the term containing it—the line-bending energy contribution—is minimized by $\psi = 1/2$. In other words, because there is a price for bending lines, the system wishes to arrange itself into an extended network of defects where there are not as many bends and in which the minimum

distance between them, ξ, is large. It is reasonable to expect, on the other hand, that the entropic contribution—see the last term in Eq. (15)—favors many, small defect loops and, indeed, this term gives a small ψ (and ξ) phase of pores.

The trends in ϕ_d and ψ (amount and topology of defects, respectively) can be followed with increasing surfactant volume fraction, ϕ. When the lamellar phase is dilute, the bilayer spacing is large and the "brake" term—the bilayer–bilayer interaction—is not as sensitive to increases in ϕ_d: at low surfactant fraction, we expect a large area fraction of defect. In this large ϕ_d regime, the defect bending price (which is cubic in ϕ_d) is important and an extended network of defects is expected: we expect the random line phase ($\psi = 1/2$). In the regime of concentrated lamellae, on the other hand, the bilayer–bilayer interactions dominate and the area fraction of defect is small; with this small ϕ_d, the entropy favors a small ψ pore phase. In summary, then, upon concentration of the lamellar phase, defects are diluted out with a concurrent evolution from a web-like (random line) pattern to an isolated pore phase. Furthermore, the only feature which destabilizes the random line phase with respect to the stripe phase is the bending cost of the former. As this price is greater at low ϕ (large ϕ_d), we expect a stable stripe phase at low ϕ, which will give way to the increasing ϕ progression just summarized. See Fig. 2(a) for a pictorial representation.

We have solved numerically the extremization equations which follow from (15) and (16), but we find it most instructive to capture these results with a simplified free-energy density, and we do this at two levels of approximation, both of which give good qualitative agreement with the numerical work. Specifically, we seek simple results regarding the δ and χ dependence of the progression stripes → random lines → pores. We begin with the following:

$$f = A(1 + \phi_d + \phi_d^2)\phi^2 - \delta\phi_d\phi + \chi\phi_d^3\phi(1 + a\eta^2 + b\eta^4) + \phi_d^2\phi(-1 - c\eta^2 - d\eta^4) \quad (17)$$

with η defined as $1/2 - \psi$. This serves for the line and pore phases while the stripe phase is given by the first four terms:

$$f_{\text{stripe}} = A(1 + \phi_d + \phi_d^2)\phi^2 - \delta\phi_d\phi. \quad (18)$$

The first four terms in (17), i.e., f_{stripe}, can be regarded as strictly phenomenological. The bilayer–bilayer interaction and its coupling to ϕ_d are given by $A(1 + \phi_d + \phi_d^2)\phi^2$: as ϕ increases, the brake on defects "turns on." The "push" for defects is provided by $-\delta\phi_d\phi$. Alternatively, these first four terms are suggested by the form of the coupling between ϕ and ϕ_d in the expansion of Eq. (15) in these quantities. We need the previously developed model, however, to establish the powers of ϕ_d in the remaining terms of (17). The expansion of these terms in even powers of the variable η, defined as $1/2 - \psi$, follows either from the free-energy density (15) or directly from the symmetry of the problem; the coefficients a, b, c, d are a consequence of the particular model used. Finally, the expansion of Eq. (15) in powers of η introduces new constant coefficients for the bending and entropic terms; division by the entropic coefficient (16 ln 2) rescales, once again, A, δ, and χ, giving Eq. (17).

4. Phase diagram and analytic results

At the first level of simplification, we proceed to minimize Eq. (17) with respect to both ϕ_d and η and generate (via the common tangent construction) a typical phase diagram with δ vs ϕ as shown in Fig. 3. Because the lamellar phase is not expected to be stable at low surfactant volume fractions (with respect to a hexagonal phase, say), we do not extend the phase diagram below $\phi = 0.4$; indeed, at low amphiphile concentrations, ϕ_d is too large to properly describe the system as lamellar. For this work the coefficient A is taken to be 10 and a, b, c, d are determined from Eq. (15) to be 8, 48, $8 - 2/\ln 2$, $48 - 52/3 \ln 2$, respectively. It is important to stress that for fixed δ and χ, the area fraction of defect decreases continuously with increasing surfactant.

The progression of phases is that which was described qualitatively. Below an easily obtainable value of ϕ which depends on δ and χ, the free-energy minimum corresponds to the random line phase for which the equilibrium value of $\eta = 0$, i.e., $\psi = 1/2$. In the pore phase, above this ϕ, η increases continuously from 0 (ψ decreases from 1/2) to give a true pore-like phase at high ϕ where the defect density is lowest. Because the stripe-phase free energy is distinct from that of the random line phase, the stripe to line transition is necessarily first order: we have coexistence between a lamellar phase with ribbon-like defect patterns and another with random channels, the latter with smaller area fraction of defect. In a sense, then, this first-order transition is from a phase with high density of defects to a more "perfect" bilayer system. The order of the line to pore transition depends on the values of δ and χ, but we have not investigated this dependence in detail. Increasing the value of χ simply decreases the slope of the lines separating the stripe-line and line-pore domains in Fig. 3: at a given δ, both stripe and random line phases survive to higher surfactant fractions.

If we use a final (the second level of) simplification, these results are most easily captured and summarized. With the assumption that the stripe-phase features determine ϕ_d^*, the equilibrium value of ϕ_d at a given ϕ, for stripe, random line, and pore phases, we obtain several simple analytic results from the free energies given by Eqs. (17) and (18)—all of which are in agreement with the results referred to above. (The reasoning behind this assumption was discussed in Sec. III A 3). For all phases, then, we will use

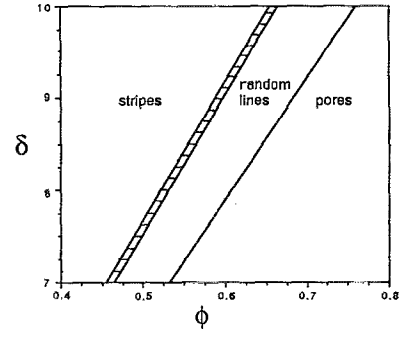

FIG. 3. Phase diagram calculated from the line defect model. Concentration of the lamellar phase decreases the defect density. $\chi = 4$ here.

$$\phi_d^* = \delta/2A\phi - \tfrac{1}{2}. \tag{19}$$

As δ becomes more positive, the area fraction of defect, ϕ_d^*, increases; as surfactant concentration increases, it decreases as required. We demand that $\phi_d^* > 0$, which imposes an upper bound on ϕ. (Alternatively, we could simply tune δ and A such that $\phi_d^* = 0$ only when $\phi = 1$, say.) Furthermore, since we have developed a small ϕ_d theory, ϕ cannot be too small. The result (19) is substituted into Eq. (18) to give the thermodynamic potential of the stripe phase, $f_{\text{stripe}}(\phi_d^*(\phi);\phi)$ (which is identical to that used to generate the phase diagram above); similarly, the general free energy of Eq. (17) is reduced to a function of η and ϕ only: $f(\phi_d^*(\phi),\eta;\phi)$.

Examination of the stripe-line stability proves to be a simple matter. For the random line phase $\eta \equiv 0$, and for the moment we assume that this phase can be described by Eq. (17). Indeed, we will see the analysis of this equation does yield the $\eta = 0$ solution. It is easy to show that the stripe phase has the lower free energy at low ϕ ($< \phi_{s-l}$) where ϕ_d is larger, and the line phase at higher ϕ ($> \phi_{s-l}$) with ϕ_d smaller. This ϕ_{s-l} at which the free energies cross is, within this simplified treatment,

$$\phi_{s-l} = \frac{\delta}{A}\left(\frac{\chi}{\chi + 2}\right), \tag{20}$$

and corresponds to

$$\phi_d^{l-s} = 1/\chi. \tag{21}$$

Again, if $\phi_d^* > \phi_d^{l-s}$, the stripe phase has the lower free-energy density. From Eq. (20) we see that as δ becomes more positive, the stripe phase survives to higher concentrations—since more defect is present for high δ, remaining in the stripe phase avoids increasing the bending cost. As χ increases, it is also expected that ϕ_{s-l} should increase, and this is indeed so. This mimics the behavior seen in phase diagrams. Again, by construction, the stripe-to-line transition is first order. We turn now to the random line to pore ($\eta > 0$) transition.

Recall the free-energy density

$$f = A(1 + \phi_d^* + \phi_d^{*2})\phi^2 - \delta\phi_d^*\phi + \chi\phi_d^{*3}\phi(1 + a\eta^2 + b\eta^4) + \phi_d^{*2}\phi(-1 - c\eta^2), \tag{22}$$

where ϕ_d^* is given by Eq. (19). Note that we have set the coefficient $d = 0$ in (17) since it can be shown that, in the case where Eq. (17) is minimized with respect to *both* η and ϕ_d, the surfactant volume fraction at which the random line phase ($\eta = 0$) ceases to be a minimum is independent of this coefficient.

Landau analysis, at fixed ϕ, and therefore, fixed ϕ_d^*, reveals that below $\phi \equiv \phi_{l-p}$, the equilibrium value $\eta^* = 0$ provides the free-energy minimum, i.e., the free-energy curvature—coefficient of η^2—is positive for $\phi < \phi_{l-p}$. As the surfactant volume fraction increases beyond ϕ_{l-p}, η^* grows continuously away from the zero value. That is, for $\phi < \phi_{l-p}$, the random line phase ($\psi = 1/2$) minimizes the free energy density, and for $\phi > \phi_{l-p}$, the pore phase ($\psi < 1/2$) grows in. This ϕ_{l-p} is easily found to be

$$\phi_{l-p} = \frac{\delta}{A}\left(\frac{\chi}{\chi + 2c/a}\right) \tag{23}$$

with the corresponding

$$\phi_d^{p-l} = c/\chi a. \tag{24}$$

If $\phi_d^* < \phi_d^{p-l}$, the pore phase is stable. Note that $\phi_{s-l} < \phi_{l-p}$: the stripe-line phase transition (or rather the crossover in their free energies) is at lower concentration than the symmetry breaking transition just discussed. Otherwise, both ϕ_{s-l} and ϕ_{l-p} have the same dependence on δ and χ and for the same reasons.

The behavior of the $\eta^* > 0$ solution is analyzed. The pore phase grows in only for $\phi > \phi_{l-p}$ and η^* is found by minimizing the free-energy density with respect to η (and ignoring the $\eta^* = 0$ solution). We obtain

$$\eta^* = \left(\frac{c}{2\chi b\phi_d^*} - \frac{a}{2b}\right)^{1/2} \tag{25}$$

for $\phi \geqslant \phi_{l-p}$ and ϕ_d^* given by Eq. (19). As ϕ increases and ϕ_d^* decreases, η^* increases, i.e., $\psi = 1/2 - \eta$ decreases—with increasing surfactant concentration, we see evolution towards isolated, pore-like defect loops.

Finally, we solve Eqs. (20) and (23) for δ and note that these describe well the δ vs ϕ phase diagram of Fig. 3:

$$\delta = A\phi_{s-l}(2/\chi + 1) \tag{26}$$

and

$$\delta = A\phi_{l-p}(2c/\chi a + 1). \tag{27}$$

These equations also summarize the phase boundary dependence on χ.

Within the framework of the line defect model, then, we predict successive phase transitions between lamellar phases characterized by different defect topologies.

B. Defect growth model

1. Description of model

We now introduce the second model. It is suggested naturally by the micellar growth and alignment work reviewed briefly in the Introduction, and gives the same qualitative picture as the line defect model. Because the details of a chosen model are not important in determining lamellar geometry and the bilayer–bilayer interactions, the results of Sec. II and the form of the interlayer repulsion, Eq. (14), are unaffected. In particular, we still have the result that lamellar phase dilution leads to an increase in the area fraction of defect.

The building block of the defect growth model is a straight line (channel) defect of constant width a and finite, but variable, length. Because this line has ends ("caps"), there is an energy price, call it ϵ, associated with them because the head-group areas of molecules in these regions are considerably smaller than the optimal. The aspect ratio of the defect—the length-to-width ratio—will be denoted by s, and if $s = 0$, we have a pore defect resulting from fusion of the end caps; this pore will have energy ϵ. As s grows away from zero, there is one-dimensional growth of the defect into the linear, narrow channel described, and it is this linear portion which provides the favored, hemicylindrical defect

lips. This provides the analogy with the micellar growth picture—entropic considerations favor many small pores (small s), while a large value for s satisfies molecular packing constraints. It is clear that if ϵ, the end energy cost, were allowed to increase sufficiently, the defects would lengthen indefinitely until we would be in a regime where the line defect model, which does not allow ends, would be more realistic. Nonetheless, the qualitative defect patterns and their evolution with the surfactant volume fraction are the same for both models.

The dimensionless energy of a single defect is

$$\text{energy/defect} = -\delta s + \epsilon, \tag{28}$$

where δ is a dimensionless line energy ($= \delta a/k_B T$ in terms of the original energy per unit length of defect), and $\epsilon = \epsilon/k_B T$ is now a dimensionless end price. This $\delta > 0$, analogous to the quantity used in the defect growth model, will serve two purposes here: first, it leads to linear defect growth, and, secondly, it is the "push" for defects as it leads to large area fraction of channels.

A bilayer will have n_d monodisperse line defects—we ignore polydispersity as a first simplification. If the area of a pore, the species defined by $s = 0$, is taken as a^2, the relation between ϕ_d, the defect area fraction, and n_d is given by

$$\phi_d = n_d(s+1)a^2/L^2, \tag{29}$$

where L^2 is the area of a bilayer. For fixed ϕ_d, the system can organize into many small defects or fewer larger ones. By restricting the orientation of the long axes of the defects to lie along two perpendicular directions, we introduce a second simplification which is known to preserve the features of the isotropic-nematic transition of a *bulk* phase of long rods.[32] Indeed, we are looking precisely for an isotropic phase of defects, with half the lines aligned in one of the allowed directions with the other half orthogonal—a situation analogous to the random line phase of the first model—and a nematic phase with essentially all defects having the same orientation. This nematic is reminiscent of the stripe phase, except that here the defects are of finite length. Because s can go to zero, we have the pore phase included as a limiting phase of the isotropic. For a pictorial sequence of these patterns, see Fig. 2(b).

In order to have a nematic phase, and its attendant loss of orientational entropy compared to the isotropic, we include "repulsive" defect–defect interactions. Two perpendicular, interacting defects will cross, and because the cross introduces regions of unfavorably high curvature, a price is introduced for each orthogonal interaction—we are focusing again on a regime where cylindrical geometry best satisfies the molecular packing requirements. (Indeed, if higher curvature than that provided by a cylindrical lip were required, a bilayer might well reassemble into discoidal micelles, but we do not consider this possibility here.) Because the number of interacting parallel defects, at least for large s and isotropic distribution, is less than the number of crossing defects, we ignore the former at this level of the model (we elaborate on this below). Recall that in the line defect model we replaced crossings with self-avoiding bends assumed to be less costly: this allowed us to fully describe the defect energies with a single line energy. In the present model, we can easily handle either type of interaction: a cross or the corresponding bends are both characterized by an interaction energy, call it χ, but, again we implicitly use the energetically favored one. In this growth model, then, alignment to the nematic is prompted by the need to avoid a large interaction cost at higher defect densities.

2. Free energies

The dimensionless free-energy density will feature five terms:

$$f = f_d + f_t + f_o + f_i + f_b, \tag{30}$$

where f_d is the defect self-energy resulting from Eq. (28), f_t is the translational entropy, f_o the orientational entropy, and f_i the defect–defect interaction term. The bilayer–bilayer interaction, f_b, is the same as for the first model and is given by Eq. (14). In general, we proceed in the same fashion as above: to derive an appropriate free energy, we use the free energy per bilayer, divide by the number of molecules in it [see Eq. (2)], and multiply the result by the surfactant volume fraction, ϕ.

The defect energy, per bilayer, is given by Eq. (28) multiplied by the number of defects, $n_d = \phi_d L^2/(s+1)a^2$. With this, and following the procedure above, we arrive at

$$f_d = \frac{C\phi_d\phi(-\delta s + \epsilon)}{(1-\phi_d)(s+1)} \tag{31}$$

with $C \equiv \Sigma/2a^2$ the same dimensionless constant as in (13).

The area fraction of defect, ϕ_d, and the aspect ratio, s, are independent variational parameters in the problem; the third one is x, the fraction of defects aligned in one of the two allowed orientations. Because of the $-\delta < 0$ term, it is clear that f_d provides for large aspect ratio (as well as large ϕ_d), and is helped in this respect by the end energy, $\epsilon > 0$. The end energy also counteracts the push for large area fraction of defect, but for large s this effect becomes unimportant. It will be seen that ϵ enters into the extremization equation determining the aspect ratio in an uninteresting fashion: it simply adds to δ.

In order to calculate f_i, we need the number of defect crossings, recalling that a cross can be replaced by two bends if this lowers the energy. A simple way to proceed is to divide the bilayer surface into N lattice sites each associated with some area. The number of crossings is then

$$n_d x \left[\frac{n_d(1-x)}{N}\right](\text{No. of interacting sites}),$$

where $n_d x$ is the number of defects in one direction and $n_d(1-x)/N$ is the probability of a defect in the perpendicular direction at any perpendicular lattice site. The "No. of interacting sites" describes the number of neighboring positions such that placement of a perpendicular defect there will result in the overlap of the two (x and $1-x$) defects. It is proportional to the excluded area of two orthogonal lines:

$$\text{No. of interacting sites} \approx \frac{(s+1)^2 a^2}{\text{area per site}}.$$

With this, Eq. (29) for the ϕ_d dependence of n_d, the definition N (area per site) $= L^2$ (where L^2 is the bilayer area),

and the usual quantity for the number of surfactants per bilayer, we obtain

$$f_i = \frac{\chi \phi_d^2 \phi x(1-x)}{1-\phi_d}, \tag{32}$$

where $\chi \equiv \chi \Sigma / 2a^2 k_B T$ (in terms of a quantity with dimensions energy per interaction) is the dimensionless bending or crossing per interaction.

Note that this result is independent of the aspect ratio of the defects; this is not the case for parallel defects, but as mentioned, since the corresponding quantity in the isotropic phase is less for the parallel case (because there are fewer interacting aligned defects at large s), we ignore it there. In the nematic, however, where $x \approx 1$, the f_i above vanishes, and, in principle, there should be a parallel interaction term. However, upon alignment, the defects are found to lengthen—this feature, analogous to the alignment-growth coupling in the micellar system, will be quantified shortly. Now, the interaction free energy in the nematic, i.e., the quantity analogous to (32), would scale as the inverse of the aspect ratio, and it would be a small quantity because of the larger s in the aligned phase. Furthermore, while it is clear that we can assign a crossing price to interacting defects, the nature of the parallel interactions is more ambiguous. Indeed, end–end interactions which can result in loss of the costly end caps can actually stabilize the nematic.

The final quantities to be determined are the orientational and translational entropies for noninteracting, "ideal" defects—the interactions are, of course, taken care of by f_i—and can be calculated simultaneously. On a lattice with N sites we randomly set down two components, $n_d x$ of which represent "centers of masses" of defects pointing in one direction and $n_d(1-x)$ representing defects aligned orthogonally. A given lattice site can be occupied by one of each species since defects can cross. The entropy is calculated from the following number of unique arrangements:

$$\Omega = \frac{(N!)^2}{(n_d x)![n_d(1-x)]!(N-n_d x)![N-n_d(1-x)]!}$$

and if $n_d \ll N$, a condition corresponding to the continuum limit, we succeed in decoupling the orientational entropy from the translational. We find, with the usual manipulations involving Stirling's formula, the free energies (with $C = \Sigma/2a^2$, as before):

$$f_t = \frac{C\phi_d \phi}{(1-\phi_d)(s+1)}\left(\ln \frac{\phi_d}{s+1} - 1\right) \tag{33}$$

and

$$f_o = \frac{C\phi_d \phi}{(1-\phi_d)(s+1)} \times [x \ln x + (1-x)\ln(1-x) + \ln 2]. \tag{34}$$

To arrive at these final results, we have used, in the quantity $\ln(n_d/N)$, the fact that the number of lattice sites is proportional to the bilayer area L^2. The resulting extra additive factor proportional to n_d is absorbed into ϵ of Eq. (31). The isotropic phase has been taken as the zero of the orientational entropy, i.e., $f_o \equiv 0$ for $x = 1/2$. Recall, from analogy with the micellar work, that f_t favors, at fixed ϕ_d, many small defects, and f_t favors an isotropic orientation.

Collecting of the free-energy-density terms gives, after division by the constant C (thereby rescaling A and χ)

$$f = \frac{A\phi^2}{(1-\phi_d)(1-\phi-\phi_d)} + \frac{\chi \phi_d^2 \phi x(1-x)}{1-\phi_d} + \frac{\phi_d \phi}{(1-\phi_d)(s+1)}\left[\ln \frac{\phi_d}{s+1} - 1 + x \ln x + (1-x)\ln(1-x) + \ln 2 - \delta s + \epsilon\right]. \tag{35}$$

In principle, since there appear three variational parameters (x, ϕ_d, s) we need to minimize this free-energy density with respect to each.

3. Results

As was done for the line defect model above, we decouple the value of ϕ_d^*, the equilibrium defect density, from the details of the patterns. δ is made large so that s becomes large, and the increase in ϕ_d is counteracted with a large A. This limit again suggests a free-energy density, given by Eq. (18), which is minimized with respect to ϕ_d yielding Eq. (19) for its equilibrium value. On the other hand, we can be more consistent with the form of the bilayer–bilayer interaction used in Eq. (35) and determine ϕ_d from $f' = A\phi^2/(1-\phi-\phi_d) - \delta\phi_d\phi$, which gives a simple result if terms linear in ϕ_d only are retained. We stress, again, that the form of the bilayer repulsive term is not important: it is just a matter of convenience to use Eq. (18) as it simplifies the analytic work leading to the construction of the phase diagram for the line defect model. With ϕ_d^* replacing ϕ_d in Eq. (35), we minimize the free-energy density with respect to x and s. The simultaneous equations are easily solved numerically, and we learn that, with increasing defect fraction, there is a strong first-order phase transition from an isotropic (random line-like) phase with $x = 1/2$ to a nematic (stripe-like) pattern with $x \lesssim 1$, as shown in Fig. 2(b). For typical values of δ and χ (ϵ simply adds to δ, as seen below), a small ($\Delta\phi < 0.01$) coexistence region in ϕ space is found (via a common tangent construction) between a lamellar phase with an isotropic defect pattern and one with oriented channels.

We can also obtain these results by using Eq. (35) with $x \equiv 1/2$ for the isotropic phase and $x \equiv 1$ for the nematic. In the isotropic phase the equilibrium aspect ratio is given by $(\partial f/\partial s)_{x=1/2} = 0$, or

$$s_I = \phi_d^* e^{\delta + \epsilon} - 1, \tag{36}$$

and this phase is stable if

$$\phi_d < \sqrt{2/\chi}\, e^{-(\delta+\epsilon)/2} \equiv \phi_d^c. \tag{37}$$

As ϕ_d^* increases—as the lamellar phase is diluted—we learn that the defects grow into longer channels: we progress away from the pore phase. When ϕ_d^* increases beyond ϕ_d^c, as given above, there is a first-order transition into the nematic phase of line defects with the aspect ratio

$$s_N = 2\phi_d^* e^{\delta + \epsilon} - 1 \tag{38}$$

as follows from solving $(\partial f/\partial s)_{x=1} = 0$. Note the alignment-growth coupling upon going from the isotropic to the oriented phase in which, for the same ϕ_d, the defects are longer. [The factor of 2 appearing in Eq. (38) results from our particular choice of restricted orientations.] As χ, the defect interaction price, is increased, the nematic phase appears at lower defect fraction and consequently survives to a higher surfactant concentration.

In summary then, for both the line defect and defect growth models, we have the following progression with concentration of the lamellar phase (corresponding to defect dilution): stripe phase (nematic) to isotropic line phase to pores. In the line model the first transition is first order by construction, and in the growth picture it corresponds to a first-order nematic-isotropic transition. Because the line to pore progression in the isotropic regime of the growth model is a one-dimensional reorganization, it cannot be a real phase transition; in the line defect work the random line to pore rearrangement corresponds to an Ising symmetry breaking ($\psi = 1/2$ to $\psi < 1/2$) transition which need not be second order in ϕ space, depending on the values of δ and χ.

IV. DISCUSSION AND CONCLUSIONS

Both models discussed above give rise to analogous patterns with change in surfactant concentration: But are the driving forces for these topological changes the same? Consider first the pore-like defects in concentrated lamellar phases. In both models these pores are entropically stabilized. With increasing defect density, the pores of the growth model elongate in one dimension to an isotropic line phase in order to take advantage of the cylindrical packing of the surfactant. In the same sense, the pore-like objects of the line model evolve into more extended line patterns, thus minimizing the number of bends, which are regions of noncylindrical packing of the surfactant—bending involves a price for deformation of the cylindrical lips. In both models, then, the progression from pore to an isotropic (random) line phase, with increasing area fraction of defect, is driven by the need to pack the maximum number of molecules with preferred curvature while still profiting from the "topological" entropy of an isotropic or random line distribution. In the growth model, this orientational entropy is given up, with the appearance of the nematic phase, only when defect–defect interactions become too costly at higher coverages. The random line phase of the first model is characterized, similarly, by defects which cover the bilayer surface, the lines bending in order to avoid interactions while trying to gain topological entropy: we assume that crossing defects cost more than the gentle bends on squares of edge length ξ. With increasing density of channels, more bends are introduced in order to prevent an increasing number of interactions, with the eventual transition to a stripe phase. In this sense, the random line to stripe transition in the line defect model, as in the growth picture, is triggered by defect interactions. The stability of the oriented phase (stripe or nematic) in both cases is controlled via the quantity χ.

Finally, it is apparent that if flexibility, along with an infinite price for the defect ends, were introduced for the defect growth model, we would recover the line defect model.

We have stressed that the presence of defects in the lamellar phase results from an attempt to satisfy molecular packing demands within the constraints of the aggregate packing required at moderate to high surfactant volume fractions. In order to make connection with the work of Sadoc and Charvolin (see Refs. 16 and 33 for a review), we note, in our work, the frustration between local, molecular forces and the large-scale liquid-crystalline order when the amphiphile molecules are packed in homogeneous, perfect bilayers. Resolution of this frustration involves allowing for some of the molecules, at least, to reside in highly curved defect lips which leads to pattern formation on the bilayer face. Similarly, in the geometrical approach of Sadoc and Charvolin, local stresses lead to frustration which is also relieved by large-scale topological reorganization of the amphiphilic system. Specifically, they begin with a stable bilayer, existing under some "experimental" conditions, in which the head and tail areas of a molecule are equal. Because the forces determining these respective areas are not the same, it can be expected that a different temperature, say, the areas will no longer be similar, thereby introducing curvature into *each monolayer*. By symmetry, both monolayers will gain either positive or negative curvature resulting in disruption of the bilayer hydrophobic core. This, then, is the frustration which leads to structural reorganization. The common feature shaped by their work and ours is a locally stressed bilayer in which the molecular packing requirements lead to a frustration. Our approach, however, explores directly the statistical thermodynamic consequences of this frustration as a function of surfactant concentration. In this same light, we comment upon additional analogies, first to the ripple phases mentioned in the Introduction, and then to the domain walls present in commensurate–incommensurate phases on surfaces.

At temperatures below which the bilayers of a lamellar phase have a fluid hydrocarbon core, phospholipid membranes may deform with a sawtooth pattern.[19–22] This ripple phase with its modulated defects arises, again, from packing competition between heads and chains; in phosphatidylcholine, for example, the head-group area is larger than that of the tails. It seems, then, that such local stress in the lamellar phase can be relieved in yet another way: through ripples. Though in our defect work we have not explicitly mentioned these packing competitions between the hydrophobic and hydrophilic portions of the molecule, it is implied that the competition is such that the entire amphiphile enjoys regions of high curvature allowing for a relatively larger head group.

Finally, consider the problem of absorbing gas atoms onto a crystal surface where the natural periods of absorbate and substrate are incommensurable or mismatched; again, a frustrated situation arises with resolution provided by domain walls separating regions of commensurate matching of the two lattices in question.[34] It turns out that under suitable conditions, if wall crossings are costly, stripe phases of these domain walls are stable. Furthermore, at finite temperature these walls fluctuate in the same way expected for the defect channels of our lamellar systems, and dislocations in these

incommensurate stripe phases can lead to more random wall patterns reminiscent of our lines phases. It seems likely that the language and the machinery of incommensurate–commensurate theory can be exploited further in our work. With this discussion of how molecular stresses lead to reorganization of the lamellar phase (except for the case just mentioned), we turn to some experimental work which renders more plausible these theoretical notions.

It is clear from the experimental papers cited in the Introduction that lamellar phases are pierced by pores or channels. We have seen that as δ, the core defect energy, becomes larger, the bilayers are more fragmented by channels. Implicit in this conclusion is the argument that surfactant molecules requiring larger curvature will be characterized by a more positive δ. Neutron scattering studies on the lamellar phase of the ternary system SdS/decanol/water[6] show that, for constant water fraction, the bilayers have a greater area fraction of defects as the surfactant/alcohol ratio is increased. Furthermore, as this ratio is increased, the periodicity of the lamellar phase decreases—indeed our model requires that the periodicity (d spacing) decrease with increasing defect density. What is happening here is clear. Both the surfactant and the alcohol have the same tail group, but the former has the larger head. As the amount of surfactant relative to decanol is increased, there is need to accommodate the larger head groups, and this promotes defects of positive curvature. Indeed, it seems that SdS molecules will be packed preferentially in the defect lips.[35] As is expected, at still higher surfactant/alcohol ratios (at constant water content), the lamellar phase is disrupted via a phase transition.

Finally, what can be said about dilution of this system at a fixed SdS/decanol ratio? Recall that we predict an increase in defect density with increasing water content. Experimentally, it is found that dilution of this system leads, by a first-order transition, to a phase of infinite ribbons arranged in a two-dimensional centered rectangular lattice.[36] Though it is not stated that the bilayer defect area fraction increases with dilution in the *lamellar* phase, it is reasonable to infer that this is the case and that the phase transition is mediated by the increasing defect density, perhaps even through our proposed stripe phase which is certainly similar to the experimental ribbon phase. Finally, we point to Helfrich's[13] analysis of the potassium caprylate/decanol/water phase diagram which can be found in the classic review by Ekwall. There it is suggested that two coexisting lamellar phases, which can be connected by a dilution path at constant surfactant/alcohol ratio, differ in that the more dilute one contains a high concentration of pores.

ACKNOWLEDGMENTS

We wish to thank Neville Boden, Jean Charvolin, Diego Kramer, Pierre Schaaf, Julian Talbot, Gordon Tiddy, Shi-Qing Wang, and Zhen-Gang Wang for many enjoyable and stimulating discussions. This work was supported by a grant (No. CHE88-16059) from the National Science Foundation and by a collaborative research award (No. 880201) from the NATO Scientific Affairs Division. The Fritz Haber Molecular Dynamics Research Center, of which A.B.S. is a member, is supported by the Minerva Gesellschaft fur die Forschung, Munich, Federal Republic of Germany. We also wish to thank the U.S.–Israel Binational Science Foundation for financial assistance.

[1] M. C. Holmes and J. Charvolin, J. Phys. Chem. **88**, 810 (1984).
[2] G. Chidichimo, L. Coppola, C. La Mesa, G. A. Ranieri, and A. Saupe, Chem. Phys. Lett. **145**, 85 (1988).
[3] M. C. Holmes, D. J. Reynolds, and N. Boden, J. Phys. Chem. **91**, 5257 (1987).
[4] P. Kekicheff, B. Cabane, and M. Rawiso, J. Phys. (Paris) Lett. **45**, 813 (1984).
[5] P. Kekicheff and G. J. T. Tiddy, J. Phys. Chem. **93**, 2520 (1989).
[6] Y. Hendrikx, J. Charvolin, P. Kekicheff, and M. Roth, Liq. Cryst. **2**, 677 (1987).
[7] P. Ekwall, in *Advanced Liquid Crystals*, edited by G. H. Brown (Academic, New York, 1975), Vol. 1.
[8] J. N. Israelachvili, D. J. Mitchell, and B. W. Ninham, J. Chem. Soc. Faraday Trans. 2 **72**, 1525 (1976); A. Ben-Shaul and W. M. Gelbart, in *Micelles, Microemulsions and Monolayers*, edited by W. M. Gelbart, D. Roux, and A. Ben-Shaul (Springer, New York, 1991).
[9] W. M. Gelbart, A. Ben-Shaul, A. Masters, and W. E. McMullen, in *Physics of Amphiphiles: Micelles, Vesicles, and Microemulsions*, edited by V. Degiorgio and M. Corti (North-Holland, Amsterdam, 1985); W. M. Gelbart, W. E. McMullen, and A. Ben-Shaul, J. Phys. (Paris) **46**, 1137 (1985); Mol. Cryst. Liq. Cryst. **132**, 325 (1986).
[10] C. Bagdassarian, W. M. Gelbart, and A. Ben-Shaul, J. Stat. Phys. **52**, 1307 (1988).
[11] R. R. Balmbra, J. S Clunie, and J. F. Goodman, Nature (London) **222**, 1159 (1969).
[12] M. Kléman, C. E. Williams, M. J. Costello, and T. Gulik-Krzywicki, Philos. Mag. **35**, 33 (1977).
[13] W. Helfrich, in *Physics of Defects*, edited by R. Balian, M. Kléman, and J. P. Poirier (North-Holland, Amsterdam, 1981).
[14] M. Allain and M. Kléman, J. Phys. (Paris) **48**, 1799 (1987).
[15] M. Kléman, Liq. Cryst. **3**, 1355 (1988).
[16] J. F. Sadoc and J. Charvolin, J. Phys. (Paris) **47**, 683 (1986).
[17] L. Paz, J. M. Di Meglio, M. Dvolaitzky, R. Ober, and C. Taupin, J. Phys. Chem. **88**, 3415 (1984).
[18] M. Allain, Europhys. Lett. **2**, 597 (1986).
[19] P. A. Pearce and H. L. Scott, Jr., J. Chem. Phys. **77**, 951 (1982).
[20] J. M. Carlson and J. P. Sethna, Phys. Rev. A **36**, 3359 (1987).
[21] J. M. Carlson, S. A. Langer, and J. P. Sethna, Europhys. Lett. **5**, 327 (1988).
[22] R. E. Goldstein and S. Leibler, Phys. Rev. Lett. **61**, 2213 (1988).
[23] A. G. Petrov, M. D. Mitov, and A. I. Derzhanski, in *Advances in Liquid Crystal Research and Applications*, edited by L. Bata (Pergamon, Oxford, 1981).
[24] A. G. Petrov, M. D. Mitov, and A. I. Derzhanski, Phys. Lett. **65A**, 374 (1978).
[25] D. Roux and C. R. Safinya, J. Phys. (Paris) **49**, 307 (1988).
[26] Y. Talmon and S. Prager, J. Chem. Phys. **69**, 2984 (1978).
[27] J. Jouffroy, P. Levinson, and P. G. de Gennes, J. Phys. (Paris) **43**, 1241 (1982).
[28] B. Widom, J. Chem. Phys. **81**, 1030 (1984).
[29] D. Andelman, M. E. Cates, D. Roux, and S. A. Safran, J. Chem. Phys. **87**, 7229 (1987).
[30] M. E. Cates, D. Roux, D. Andelman, S. T. Milner, and S. A. Safran, Europhys. Lett. **5**, 733 (1988).
[31] W. Helfrich, Z. Naturforsch. **28c**, 693 (1973).
[32] R. Zwanzig, J. Chem. Phys. **39**, 1714 (1963).
[33] J. Charvolin, in *Phase Transitions in Soft Condensed Matter*, edited by T. Riste and D. Sherrington (Plenum, New York, 1989).
[34] S. N. Coppersmith, D. S. Fisher, B. I. Halperin, P. A. Lee, and W. F. Brinkman, Phys. Rev. B **25**, 349 (1982).
[35] Y. Hendrikx, J. Charvolin, and M. Rawiso, J. Colloid Interface Sci. **100**, 597 (1984).
[36] Y. Hendrikx and J. Charvolin, J. Phys. (Paris) **42**, 1427 (1981).